CHARACTERIZATION OF MESOSTASIS AREAS IN MARE BASALTS: PETROGRAPHY AND MINERAL CHEMISTRY. A. A. Griffiths[1,2], J. J. Barnes[2,3], R. Tartèse[2], N. J. Potts[2,4], M. Anand[2,3,*]. [1]School of Earth, Atmospheric and Environmental Science, University of Manchester, M13 9PL, UK. [2]Department of Physical Sciences, The Open University, Milton Keynes, MK7 6AA. [3]Department of Earth Sciences, The Natural History Museum, Cromwell Road, London, SW7 5BD. [4]Faculty of Earth and Life Sciences, VU University Amsterdam, NL *Correspondence: Mahesh.Anand@open.ac.uk

Introduction: Mare deposits account for ~ 20 % of the lunar surface [1] and represent a significant proportion of samples returned from the near-side of the Moon by the Apollo missions. Although volumetrically insignificant (accounting for < l % of the lunar crust [2]), mare volcanic samples are the only samples providing information about the lunar mantle. Mare basalts are generally classified into three main groups based on their bulk-rock TiO_2 contents: very-low-Ti, low-Ti, and high–Ti. Further subdivisions have been proposed based on bulk Al_2O_3 and K_2O contents [e.g., 2]. Whilst the mineralogy and geochemistry of mare basalts have been well documented, detailed characterization of mesostasis areas within them has been largely overlooked. Mesostasis areas consist of the crystallization products of late-stage melt pockets, trapped between the interstices of earlier-formed crystals of major minerals, forming a complex mixture of fine-grained minerals and glass [2]. These mesostasis areas can notably contain phases rich in incompatible elements, including volatiles, such as apatite [e.g., 2-4].

In this study we examined mesostasis areas in four Apollo mare basalts: 10044, a coarse-grained high-Ti basalt; 12064, a coarse-grained low-Ti basalt; 15058, a coarse-grained pigeonite low-Ti basalt; and 70035, a medium-grained high-Ti basalt [5].

Methods: A FEI Quanta 3D dual beam Scanning Electron Microscope (SEM) located at The Open University was initially used to acquire X-ray element maps for each sample. Elemental mapping was carried out using an electron beam current of 0.6 nA and an accelerating voltage of 20.05 kV. Mesostasis areas were identified using a combination of element maps and back scatter electron (BSE) images (e.g., Fig. 1). Quantitative analyses of individual minerals in and around mesostasis areas were performed using a Cameca SX100 Electron Microprobe (EMP) at The Open University. Typical analytical conditions included an accelerating voltage of 20 kV and a beam current of 20 nA. Most phases were analyzed using a beam of 1-5 μm diameter except plagioclase and glasses that were typically analyzed using a beam size of 5-10 μm to minimize any potential volatilization of Na and K.

Results: Texturally, the mesostasis areas observed in samples 10044 and 12064 are more coarse-grained compared to those in 15058 and 70035. The mesostasis areas in 15058 and 70035 are patchy and dispersed, being generally smaller in size (typically 50 to 100 μm wide) than those in the other two samples (> 100 μm, typically ~ 200 μm). In general, the mesostasis areas across all samples consist of an assemblage of silica, glass, fayalitic olivine, troilite, pyroxene, phosphates, ilmenite and symplectite assemblages, consisting of fayalite, silica and hedenbergite, formed by the breakdown of pyroxferroite giving rise to a Swiss-cheese texture [e.g., 6]. Olivine in mesostasis in 10044 and 12064 is closely associated with fine-grained blebs of glass. No pyroxferroite or symplectite was observed in samples 15058 and 70035. Among the four samples, 70035 contains the highest proportion of glass.

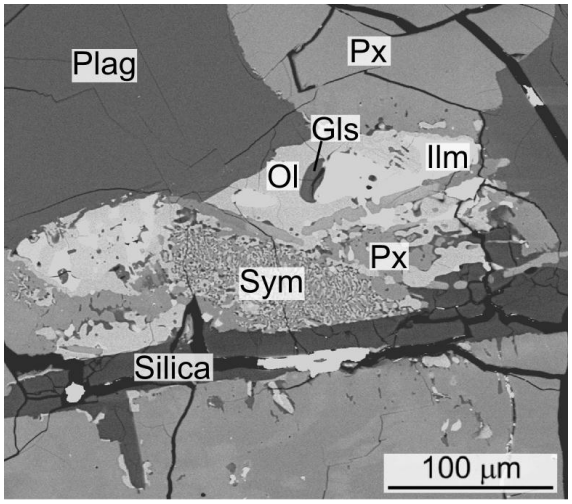

Figure 1: BSE image of a mesostasis area in basalt 12064. Plag = plagioclase, Px = pyroxene, Gls = glass, Ol = olivine, Ilm = ilmenite, Sym = symplectite assemblage of fayalite-silica-hedenbergite.

Except for sample 70035, a notable characteristic of mesostasis in the other three samples is in terms of extreme Fe-rich pyroxene compositions that plot close to Fe-Hd join in the pyroxene quadrilateral (Fig. 2). The compositions of pyroxenes in mesostasis areas of sample 70035, on the other hand, display much less Fe-enrichments and are compositionally similar to non-mesostasis pyroxenes in mare basalts (Fig. 2).

In all four samples the composition of plagioclase feldspar show relatively restricted range from An_{70} to An_{90}. Plagioclase grains located inside mesostasis areas are more sodic, with slightly elevated Fe contents,

compared to the grains outside of the mesostasis areas that are more anorthitic. Some mesostasis areas also contain K-feldspar. Olivine was only observed in the mesostasis of samples 10044 and 12064, and is fayalitic in composition (Fo_{0-5}). Ilmenite and silica compositions are very uniform in all the samples studied, irrespective of whether they occur inside or outside the mesostasis areas.

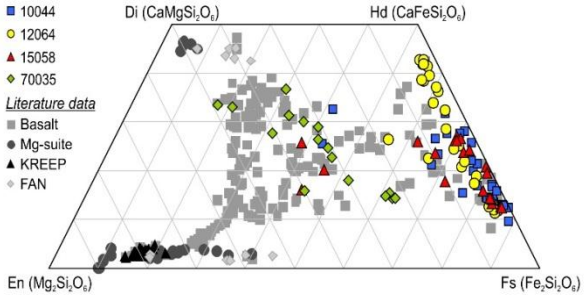

Figure 2: Pyroxene quadrilateral displaying composition of pyroxenes in the studied mesostasis areas. For comparison, the compositions of pyroxenes in mare basalts, Mg-suite, KREEP, and ferroan anorthosites are also plotted [compilation of pyroxene compositions courtesy of K. H. Joy].

In addition to silicate minerals, pockets of glass were also analyzed, and were found to be mostly of two types: Si-rich and K-rich glasses. The mesostasis glass compositions show striking resemblance to the composition of lunar granites on a total alkali versus silica diagram (Fig. 3).

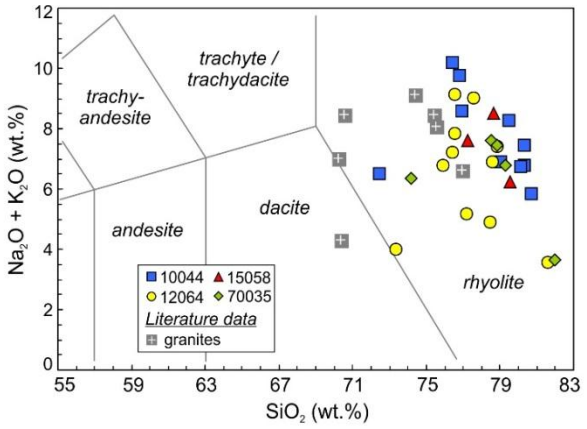

Figure 3: Total alkali versus silica diagram showing the glass compositions measured in the mesostasis areas. Data for lunar granites [7] have been plotted for comparison.

Discussion: The results presented in this study highlight the similarities and differences in mineralogy and geochemistry of mesostasis areas in four Apollo mare basalts. Pyroxene compositions are typical for mare basalts with most of the pyroxene compositions in mesostasis areas in 10044, 12064 and 15058 showing extreme Fe-enrichments. These compositions are consistent with the common fractionation trends exhibited by mare basalts (Fig. 2; [e.g., 8-9]). However, the mesostasis pyroxene compositions in 70035 are more Mg-rich compared to those in the other high-Ti basalt 10044. Given that these are both high-Ti basalts could indicate that either we did not analyze pyroxenes within "true" mesostasis areas in 70035 or that conditions of crystallization were different between the two samples. The latter would be consistent with the observation that sample 70035 contains abundant glass which could be a result of relatively rapid cooling of late-stage melt pockets, compared to those in the other three samples. Rapid cooling is likely to have prevented establishment of extreme fractionation trends reflected by pyroxene compositions, as seen in the case of other samples.

Overall, the glass compositions among all mesostasis areas are silica saturated (Fig. 3). They essentially represent pockets of residual melt, evolved from basaltic melts that underwent fractional crystallization, resulting in melt compositions similar to lunar granites [7].

We are conducting additional studies focusing on recalculating the bulk-compositions of mesostasis areas by combining modal mineralogy and quantitative mineral data, followed by melt modelling in order to further constrain the melt compositions from which apatite typically crystallizes in mare basalts [10]. This will allow a better assessment of the volatile inventory of mare basalt source regions through apatite analyses.

Acknowledgments: The Paneth Trust for Meteorites Research is thanked for a bursary awarded to MA, which funded AAG for a summer internship at the Open University. We also thank NASA CAPTEM for allocation of Apollo samples to MA.

References: [1] Whitten J. et al. (2011) *JGR, 116*, E6. [2] Taylor G. J. et al. (1991) *Lunar Sourcebook*, 183-284. [3] McCubbin F. M. et al. (2011) *GCA, 75*, 5073-5093. [4] Tartèse R. et al. (2013) *GCA, 122*, 58-74. [5] Meyer C. (2011) *Lunar Sample Compendium*. [6] Ware N. G. and Lovering J. F. (1970) *Science, 167*, 517-520. [7] Seddio S. M. et al. (2013) *Am. Mineral., 98*, 1697-1713. [8] Anand M. et al. (2006) *GCA, 70*, 246-264. [9] Joy K. H. et al. (2008) *GCA, 72*, 3822-3844. [10] Potts N. J. et al. (2014) *LPS XLIV* (this meeting).